Structural changes and ferroelectric properties of $BiFeO_3-PbTiO_3$ thin films grown via a chemical multilayer deposition method

Cite as: J. Appl. Phys. **105**, 014101 (2009); https://doi.org/10.1063/1.3053773
Submitted: 21 August 2008 . Accepted: 09 November 2008 . Published Online: 05 January 2009

Shashaank Gupta, Ashish Garg, Dinesh Chandra Agrawal, et al.

Structural changes and ferroelectric properties of $BiFeO_3-PbTiO_3$ thin films grown via a chemical multilayer deposition method

Shashaank Gupta,[1] Ashish Garg,[2,a)] Dinesh Chandra Agrawal,[1]
Shuvrajyoti Bhattacharjee,[3] and Dhananjai Pandey[3]
[1]*Materials Science Programme, Indian Institute of Technology, Kanpur 208016, India*
[2]*Materials and Metallurgical Engineering, Indian Institute of Technology, Kanpur 208016, India*
[3]*School of Materials Science and Technology, Institute of Technology, Banaras Hindu University, Varanasi 221005, India*

(Received 21 August 2008; accepted 9 November 2008; published online 5 January 2009)

Thin films of $(1-x)BiFeO_3-xPbTiO_3$ (BF-xPT) with $x \approx 0.60$ were fabricated on Pt/Si substrates by chemical solution deposition of precursor BF and PT layers alternately in three different multilayer configurations. These multilayer deposited precursor films upon annealing at 700 °C in nitrogen show pure perovskite phase formation. In contrast with the equilibrium tetragonal structure for the overall molar composition of BF:PT::40:60, we find monoclinic structured BF-xPT phase of M_A type. Piezoforce microscopy confirmed ferroelectric switching in the films and revealed different normal and lateral domain distributions in the samples. Room temperature electrical measurements show good quality ferroelectric hysteresis loops with remanent polarization P_r of up to 18 $\mu C/cm^2$ and leakage currents as low as 10^{-7} A/cm^2. © *2009 American Institute of Physics*.
[DOI: 10.1063/1.3053773]

I. INTRODUCTION

$BiFeO_3$ (BF), a multiferroic material showing the coexistence of ferroelectric and magnetic orderings in the same phase, is the most studied multiferroic material since the report of the existence of very large polarization in epitaxial BF thin films.[1] It shows a ferroelectric-paraelectric transition at ~1103 K (Ref. 2) and a G-type antiferromagnetic-paramagnetic transition at ~643 K with an incommensurate spiral magnetic ordering.[3] It possesses a rhombohedrally distorted perovskite structure with space group $R3c$ at room temperature.[4] Recently, it has been shown to exhibit a series of other transitions: existence of a β-phase between 820 and 925 °C, followed by the presence of a γ-phase between 925 and 933 °C,[5] a spin-glass transition at 120 K, and a ferromagnetic transition at 5 K.[6] Studies on single crystals have shown very high values of polarization, close to 100 $\mu C/cm^2$.[7] However, polycrystalline BF ceramics and films have often been plagued by high electrical conductivity due to which hysteresis loops appear leaky. This is believed to be due to the presence of various secondary phases and valence fluctuations at the Fe site (Fe^{3+} and Fe^{2+}) during processing.[8,9]

Solid solution of BF with insulating ABO_3 perovskite oxides, such as $PbTiO_3$ (PT) (Ref. 10) and $BaTiO_3$,[11] has been suggested as one of the alternatives to improve the electrical resistance of the material. Among these, the mixed $(1-x)BiFeO_3-xPbTiO_3$ (BF-xPT) system is very interesting, as it not only forms a continuous solid solution but also exhibits a morphotropic phase boundary (MPB) (Ref. 12) with a narrow composition width $\Delta x \approx 0.03$, in which the tetragonal (T) and rhombohedral (R) phases coexist.[13] Outside the MPB region, only the T and R phases are observed for $x \geq 0.31$ and $x \leq 0.27$, respectively.[13] This solid solution system is also attractive because of the high ferroelectric Curie temperature in the range of 763–1100 K (Ref. 12) and unusually large tetragonality $[\eta=(c/a)-1=0.187$, i.e., 18.7%] for $x=0.31$,[13,14] which is three times that in PT. These features have led to the many studies on BF-xPT films in the past few years where films have shown good low temperature ferroelectric properties.[15–20] However, none of these studies report good quality room temperature ferroelectric hysteresis loops, especially at frequencies below 1 kHz, presumably due to high intrinsic leakage.

Here, we report on the structural changes and insulation resistance of BF-xPT thin films with $x \approx 0.60$ obtained by a multilayer deposition approach involving spin coated precursor layers of BF and PT of varying thicknesses and number of bilayers on the Pt/Si substrates. In contrast with the expected tetragonal structure, as reported in the bulk samples of the same composition,[12] the structure of these films is found to be monoclinic. These films show reasonably high remanent polarization at room temperature with excellent leakage characteristics.

II. EXPERIMENTAL DETAILS

A 0.15M BF precursor solution was prepared by first dissolving high purity bismuth nitrate pentahydrate and iron (III) nitrate nonahydrate in glacial acetic acid and 2-methoxyethanol, respectively, followed by mixing of the two solutions and further addition of acetic anhydride and a few drops of ethanolamine for stabilization. This solution was subsequently stirred for 3 h. Similarly, a 0.15M PT precursor solution was prepared by dissolving lead (II) acetate trihydrate in glacial acetic acid followed by dropwise addition of titanium (IV) butoxide (stabilized with acetyl acetonate) and subsequent stirring for 3 h. The precursor PT and

a)Electronic mail:a.garg.98@gmail.com.

BF layers were alternately deposited on platinized-Si substrates by spin coating at a speed of 4000 rpm for 30 s. After each coating, the films were dried for 12 min at 360 °C, followed by deposition of the next layer. Finally after completion of deposition, the whole stack was annealed at 700 °C for 1 h in nitrogen atmosphere. Three different types of layered configurations were synthesized: BFPT16, BFPT8, and BFPT4. BFPT16 contains 16 bilayers of BF and PT of ~10 and ~20 nm each, BFPT8 contains 8 bilayers of ~20 nm thick BF and ~40 nm thick PT, and BFPT4 contains 4 bilayers of ~40 nm thick BF and ~80 nm thick PT. The overall stack thickness was maintained at ~480–500 nm for all the three configurations. In all configurations, the PT layer was deposited before the BF layers. The average composition of these films corresponds to $x = 0.60$.

The thickness of the films was measured by a Tencor Alpha X-100 profilometer. Thermoelectron ARL X'tra x-ray diffractometer was used for collecting powder x-ray diffraction (XRD) data. The package FULLPROF (Ref. 21) was used for Le-Bail refinements using the XRD data in the 2θ range of 15°–120°. In the refinements, the data in the 2θ ranges of 36°–43.3° and 85°–88° were excluded due to strong texture effects and the substrate peaks. Further, coexistence of Pt (fcc) substrate peaks was also taken into account in the refinements.

Scanning electron microscope (SEM) (Zeiss SUPRA™ 40 VP) was used for microstructure and compositional studies. The contact mode piezoresponse force microscopy (PFM) studies were carried out using a scanning probe microscope (NT-MDT Solver). Magnetic measurements were carried out using a vibrating sample magnetometer (ADE-DMS EV-7VSM) at room temperature. 200 μm diameter platinum electrodes were sputter deposited on the films to facilitate the electrical measurements. The ferroelectric properties of the films were measured by Radiant Precision *LC* ferroelectric tester. Current-voltage characteristics were measured by Keithley 6517A electrometer.

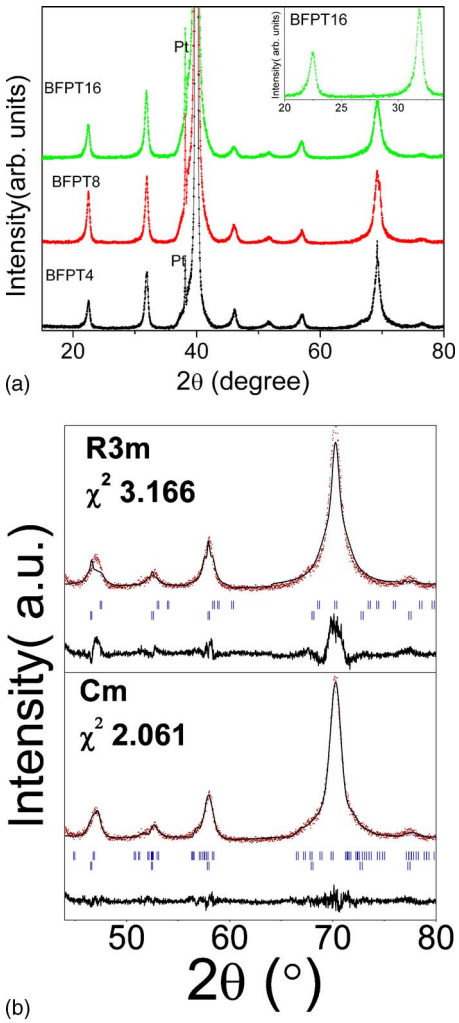

FIG. 1. (Color online) (a) Powder XRD patterns of BFPT16, BFPT8, and BFPT4. The inset shows zoomed 100 and 110 pseudocubic profiles for BFPT16 (b) The LeBail fits for the XRD data of BFPT16 using *R*3*m* and *Cm* space groups. The dots represent the observed data, while the continuous line represents the calculated profiles. The bottom plot is the difference profile. The upper and lower sets of bars above the difference profiles correspond to Bragg peaks for BFPT and Pt, respectively.

III. RESULTS AND DISCUSSION

A. Structural characterization

Grazing angle XRD patterns of the three samples in the 2θ range of 15°–80° are shown in Fig. 1(a). The patterns do not show the presence of individual peaks of PT and BF suggesting intermixing of these during postdeposition heat treatment and formation of a solid solution. This also indicates that the XRD peaks in Fig. 1(a) belong to BF-0.60PT solid-solution phase only. In order to verify the compositional variations across the thickness of the films, cross-sectional SEM was performed on all the samples and a representative micrograph of a BFPT16 sample (having thinnest bilayers) is shown in Fig. 2. The micrograph does not show any contrast between individual BF and PT layers, suggesting intermixing between them. The image also shows that the film thickness was reasonably uniform. Further, EDAX measurements showed that the films contain approximately 60% PT. Although these observations appear to be in agreement with the XRD results showing a single phase material, local compositional gradients cannot be ruled out due to insufficient resolution of SEM image and errors associated with EDAX measurements.

For the average nominal composition BF-0.60PT of these films, the structure should be tetragonal in the *P*4*mm* space group. However, the patterns shown in Fig. 1(a) do not match with tetragonal BF-xPT but show some resemblance with the rhombohedral structure of BF-xPT. For example, the

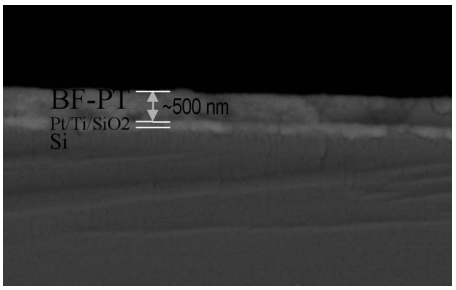

FIG. 2. Cross-sectional backscattered SEM image of a BFPT16 sample.

TABLE I. Refined cell parameters for the three films (BFPT16, BFPT8, and BFPT4) obtained by LeBail refinement with *Cm* space group.

Sample	a_m (Å)	b_m (Å)	c_m (Å)	β (deg)
BFPT16	5.456(1)	5.525(9)	4.0373(3)	90.72(2)
BFPT8	5.409(1)	5.5056(7)	4.0385(3)	90.94(2)
BFPT4	5.385(1)	5.488(2)	4.037(1)	91.18(2)

110 pseudocubic peak, which occurs around $2\theta=32.5°$ is supposed to be a doublet for the tetragonal structure with the stronger 101 peak occurring on the lower 2θ angle side while the weaker 110 peak on the higher side. The observed 110 pseudocubic peak profile does not show such a splitting. On the contrary, it shows an asymmetric tail toward the lower 2θ side suggesting the presence of a weak reflection overlapping with the stronger one on the higher 2θ angle side. This particular feature supports rhombohedral structure but then the 100 pseudocubic peak near $2\theta=23°$ should have been a singlet. The fact that this peak shows a pronounced asymmetric tail on the lower 2θ side suggests the presence of two overlapping peaks which in turn rules out rhombohedral structure as well. Monoclinic phases in the *Cm* and *Cc* space groups have been recently reported in $Pb(Zr,Ti)O_3$ (PZT) ceramics.[22,23] It has also been shown that the so-called rhombohedral compositions in *R*3*m* and *R*3*c* space group of PZT are also monoclinic in *Cm* and *Cc* space groups, respectively.[23,24]

To correctly predict the structure of the BF-0.60PT films, we further carried out the refinement of the XRD data by LeBail technique considering rhombohedral and monoclinic structures in the *R*3*m* and *Cm* space groups, respectively. We did not consider *R*3*c* and *Cc* space groups, as these are not distinguishable from *R*3*m* and *Cm* space groups, respectively, using x-ray powder diffraction data from thin films, because of the extremely low intensities of the characteristic superlattice reflections resulting from the antiphase rotation (tilting) of oxygen octahedra about one of the pseudocubic ⟨111⟩ directions in the neighboring perovskite cells. In fact, these superlattice reflections are not discernible in Fig. 1(a). The fits for a few selected profiles, as obtained from the full pattern LeBail refinement in the 2θ range of $15°-120°$, are shown in Fig. 1(b) for the two structural models. The upper and lower rows of the vertical bars below the fitted profiles correspond to the perovskite and Pt peaks. It is evident from this figure that the rhombohedral space group cannot account for the observed profiles, as it gives rise to huge mismatch between the observed and calculated profiles. The fit for the monoclinic structure, on the other hand, is very good, as indicated by significantly lower χ^2 values also. The refined cell parameters of the monoclinic phase for the films (BFPT4, 8, 16) are given in Table I. These cell parameters suggest that this monoclinic phase is of M_A type (in the notation of Vanderbilt and Cohen)[25] similar to that reported in PZT.[22,23] A monoclinic structure of M_A type has previously been reported for epitaxial BF films[1] and its presence in thin films has been attributed to the strain effects.[1]

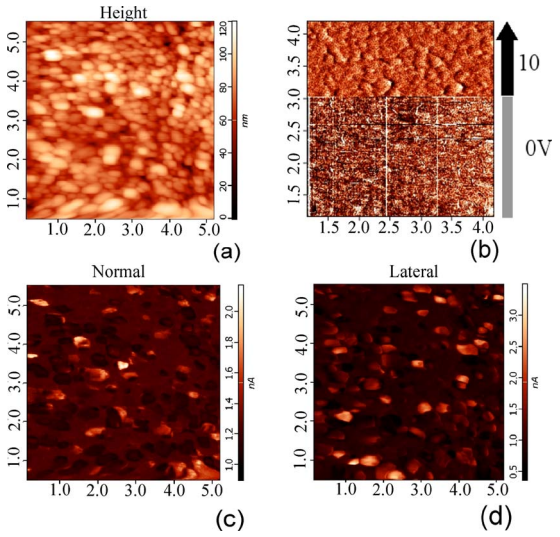

FIG. 3. (Color online) (a) Contact mode AFM image of a BFPT16 film. (b) PFM image showing the difference in contrast upon application of voltage. (c) Normal domain distribution and (d) lateral domain distribution in BFPT 16 sample.

B. Electrical characterization

The contact topography image obtained on BFPT16 sample shows an average grain size of about 200 nm [see Fig. 3(a)]. Similar microstructures and grain sizes were observed in other samples. All the samples showed piezoresponse, as confirmed by recording images with and without voltage applied to the AFM tip. PFM contrast appeared only after voltage was applied to the tip [see Fig. 3(b)]. PFM measurements on the three samples revealed the presence of both normal and lateral domains with different distributions over the sample surface analyzed, as shown in Figs. 3(c) and 3(d) for BFPT16. The measurements were made at 15 V bias and 150 kHz modulation frequency. The presence of both normal and lateral domain structures is indicative of ferroelectric switching in the films. The brighter regions in these images are representative of high piezoactivity, while darker regions indicate regions of low piezoactivity. In the normal piezoresponse images [Fig. 3(c)], the bright and dark contrast regions represent the downward and upward deflections caused by domain polarization along the *z*-axis, while in the lateral piezoresponse images shown in Fig. 3(d), the bright and dark areas correspond to the lateral deflections of the domains.[26] The medium contrast regions represent grains possessing weak piezoelectric response due to the deviation of the polarization vector away from the direction normal to the film plane.

Room temperature electrical measurements were conducted on all the three samples. Figure 4 shows the ferroelectric hysteresis loops for the three samples. The measurements were made at a frequency of 1 kHz under a bipolar electric field. The loops were not leaky as evidenced by their saturated nature. The samples were able to withstand fields above 800 kV/cm, suggesting highly insulating behavior of all the films. The polarization ($2P_r$) values were $\sim 36\ \mu C/cm^2$ for BFPT16 and decreased to $\sim 30\ \mu C/cm^2$ for BFPT4 and $\sim 16.5\ \mu C/cm^2$ for BFPT8. Saturated hysteresis loops have been previously seen in undoped BF-*x*PT

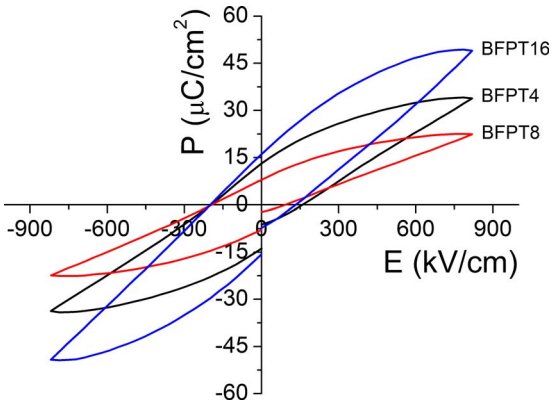

FIG. 4. (Color online) Ferroelectric hysteresis loops of BFPT4, BFPT8, and BFPT16 samples.

system but at temperatures much lower than room temperature at which the hopping conductivity is drastically suppressed.[15,19] Good quality room temperature ferroelectric hysteresis loops with higher remnant polarization have been reported in bulk La-doped BF-*x*PT,[27] but not in pure, undoped BF-xPT films. The presence of good quality loops in our samples can be attributed to our processing technique (multilayer deposition) which also led to a structural change observed in the present study. The M_A type monoclinic structure of BFPT would have polarization vector which can rotate continuously on a (110) type pseudocubic plane in contrast to the tetragonal structure whose polarization vector is constrained along the ⟨100⟩ pseudocubic direction. The ability of the polarization vector to rotate continuously on a given plane offers easier alignment of dipoles upon switching.[22,23,25] The different polarizations of three samples can be attributed to minor changes in the structural parameters of three samples (see Table I), possibly related to subtle compositional changes across the film thickness.

The results of dc leakage measurements on these three samples are shown in Fig. 5. The figure shows that the values of leakage current are below 10^{-5} A/cm^2 in our multilayer BFPT16 samples and below 10^{-6} A/cm^2 for both BFPT4 and BFPT8 samples at 300 kV/cm. These leakage current values are significantly lower as compared to the reported room temperature values for most polycrystalline $BiFeO_3$

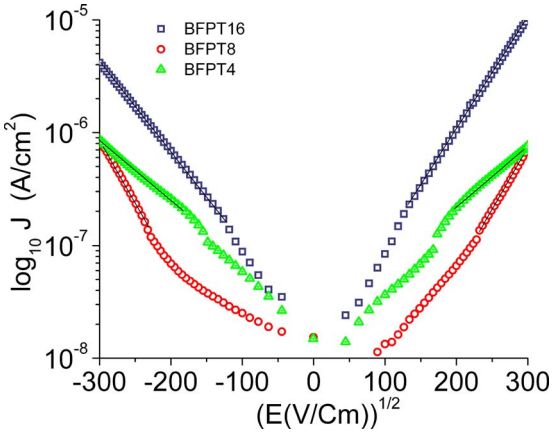

FIG. 5. (Color online) Leakage characteristics of the BFPT4, BFPT8, and BFPT16 samples.

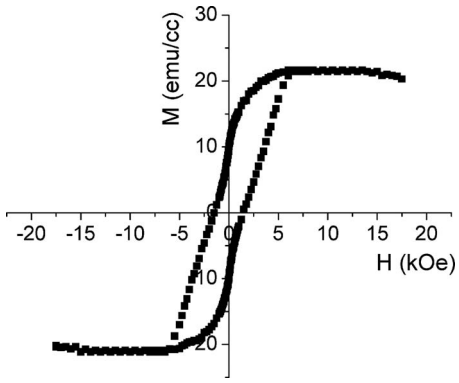

FIG. 6. Room temperature magnetic hysteresis measurements on BFPT16 sample (M: magnetization; H: applied field).

thin films[28,29] and most BF-*x*PT films reported thus far.[15,17,19,30,31] Figure 5 shows that at high fields, a relationship of the form $\log_{10} J \propto E^{1/2}$ exists suggesting bulk dominated conduction i.e., Poole–Frenkel effect. This highly insulating behavior appears to stem from the incorporation of PT into BF via a layered approach which reduces the large scale transport of the carriers or charged defects. We find the significant role of PT precursor layer, which was always deposited first on the Pt/Si substrate. The advantageous role of such a PT-buffered layer has already been demonstrated by us[20] even for the normal chemical solution deposited (without multilayer deposition approach) BF-*x*PT films where we showed that when BFPT film is deposited without first growing a PT layer, the properties remain inferior. PT, intrinsically being a better insulator than BF, may reduce the transport of charge carriers to the electrodes and hence improve the leakage characteristics. High resistivity of the samples also suggests that samples do not possess significant amount of conducting secondary phases or mixed valence states of Fe.

C. Magnetic measurements

Preliminary studies also reveal a saturated magnetic hysteresis loop depicting high magnetization in these films. For instance, Fig. 6 shows the room temperature magnetic hysteresis loop of a BFPT 16 sample showing remnant magnetization (M_r) of ~0.13 μ_B/f.u.. which is considerably large as compared to zero for single crystal $BiFeO_3$.[7] Previous studies have shown that finite magnetization is achievable in BF by melting the spiral spin cycloid via application of large enough magnetic fields,[32] substrate induced constraints in epitaxial $BiFeO_3$ thin films,[1] or by means of chemical substitutions.[12,33] In the present samples, high magnetic moment could possibly be due to thin film clamping effect, presence of PT in the solid solution, or structural change or their combination. Initial investigations on BF-*x*PT suggest that the magnetization initially increases up to ~50% PT, followed by a decrease at higher BF contents. This indirectly suggests that magnetization is likely to be due to intrinsic effects, e.g., ordering of Fe^{3+} and Fe^{+2} ions in the lattice. However, more work is needed to understand whether or not magnetic impurities such as γ-Fe_2O_3, not detectable in the XRD data, are responsible for the observed magnetization.

IV. CONCLUSIONS

In summary, BF-0.60PT films with high insulation resistance and high polarization at room temperature were fabricated via a multilayer approach using chemical solution deposition method. The structure of the resulting thin films was found to be monoclinic, in contrast to the tetragonal structure predicted by the overall stoichiometry for bulk samples. Piezoforce microscopy confirmed the presence of ferroelectric switching in the samples. Maximum remnant polarization is achieved in case of bilayer thickness of ~30 nm and is possibly due to improved intermixing of the layers. The samples also show switching up to very high fields (~800 kV/cm) and leakage currents as low as 10^{-7} A/cm^2. Our work demonstrates that it is possible to make highly insulating $BiFeO_3$–$x$$PbTiO_3$ films via a multilayer chemical solution deposition approach.

ACKNOWLEDGMENTS

A.G. thanks Department of Science and Technology and Defense Research and Development Organization (both Government of India) for Ramanna fellowship and the financial support.

[1]J. Wang, J. B. Neaton, H. Zheng, V. Nagarajan, S. B. Ogale, B. Liu, D. Viehland, V. Vaithyanathan, D. G. Schlom, U. V. Waghmare, N. A. Spaldin, K. M. Rabe, M. Wuttig, and R. Ramesh, Science **299**, 1791 (2003).
[2]W. Kaczmarek, Z. Pajak, and M. Polomska, Solid State Commun. **17**, 807 (1975).
[3]I.Sosnowska, T.P. Neumaien, and E. Steichek, J. Phys. C **15**, 4835 (1982).
[4]C. Michel, J.-M. Moresu, G. D. Achenbechi, R. Gerson, and W. J. James, Solid State Commun. **7**, 701 (1969).
[5]R. Palai, R. S. Katiyar, H. Schmid, P. Tissot, S. J. Clark, J. Robertson, S. A. T. Redfern, G. Catalan, and J. F. Scott, Phys. Rev. B **77**, 014110 (2008).
[6]M. K. Singh, W. Prellier, M. P. Singh, R. S. Katiyar, and J. F. Scott, Phys. Rev. B **77**, 144403 (2008).
[7]D. Lebeugle, D. Colson, A. Forget, and M. Viret, Appl. Phys. Lett. **91**, 022907 (2007).
[8]J. R. Teague, R. Gerson, and W. J. James, Solid State Commun. **8**, 1073 (1970).
[9]V. R. Palkar, J. John, and R. Pinto, Appl. Phys. Lett. **80**, 1628 (2002).
[10]R. T. Smith, G. D. Achenbach, R. Gerson, and W. J. James, J. Appl. Phys. **39**, 70 (1968).
[11]M. M. Kumar, A. Srinivas, and S. V. Suryanarayana, J. Appl. Phys. **87**, 855 (2000).
[12]S. A. Fedulov, P. B. Ladyzhynskii, I. L. Pyatigorskaya, and Yu. N. Venentsev, Sov. Phys. Solid State **6**, 375 (1964).
[13]S. Bhattacharjee, S. Tripathi, and D. Pandey, Appl. Phys. Lett. **91**, 042903 (2007).
[14]V. V. S. S. Sai Sunder, A. Halliyal, and A. M. Umarji, J. Mater. Res. **10**, 1301 (1995).
[15]W. Sakamoto, H. Yamazaki, A. Iwata, T. Shimura, and T. Yogo, Jpn. J. Appl. Phys., Part 1 **45**, 7315 (2006).
[16]J. R. Cheng and L. E. Cross, MRS Symposia Proceedings No. 784 (Materials Research Society, Pittsburgh, 2004), p. C8.16.1.
[17]L. Hongri, L. Zuli, L. Qing, and Y. Kailun, J. Phys. D **39**, 1022 (2006).
[18]S. H. Kang, C. W. Ahn, H. J. Lee, I. W. Kim, and J. S. Lee, J. Korean Phys. Soc. **49**, S612 (2006).
[19]M. A. Khan, T. P. Comyn, and A. J. Bell, Appl. Phys. Lett. **91**, 032901 (2007).
[20]A. Garg, S. Kar, D. C. Agrawal, S. Bhattacharjee, and D. Pandey, e-print arXiv:0804.1611v1.
[21]J. Rodriguez-Carvajal, FULLPROF, Laboratory Leon Brillouin _CEA-CNRS_CEA/Saclay, 91191 Gif sur Yvette Cedex, France, 2006.
[22]B. Noheda, J. A. Gonzalo, R. Guo, S.-E. Park, L. E. Cross, D. E. Cox, and G. Shirane, Phys. Rev. B **61**, 8687 (2000).
[23]D. Pandey, A. K. Singh, and S. Baik, Acta Crystallogr., Sect. A: Found. Crystallogr. **A64**, 192 (2008).
[24]A. K. Singh, D. Pandey, S. Yoon, S. Baik, and N. Shin, Appl. Phys. Lett. **91**, 192904 (2007).
[25]D. Vanderbilt and M. H. Cohen, Phys. Rev. B **63**, 094108 (2001).
[26]A. Gruverman, O. Auciello, and H. Tokumoto, Annu. Rev. Mater. Sci. **28**, 101 (1998).
[27]J. Cheng, S. Yu, J. Chen, Z. Meng, and L. E. Cross, Appl. Phys. Lett. **89**, 122911 (2006).
[28]Y.-H. Lee, J.-M. Wu, Y.-L. Chueh, and L.-J. Chou, Appl. Phys. Lett. **87**, 172901 (2005).
[29]H. Naganuma and S. Okamura, J. Appl. Phys. **101**, 09M103 (2007).
[30]S. W. Yu, R. Chen, G. J. Zhang, J. R. Cheng, and Z. Y. Meng, Appl. Phys. Lett. **89**, 212906 (2006).
[31]M. A. Khan, T. P. Comyn, and A. J. Bell, Appl. Phys. Lett. **92**, 072908 (2008).
[32]A. M. Kadomtseva, A. K. Zvezdin, Yu. F. Popov, A. P. Pyatakov, and G. P. Vorob'ev, JETP Lett. **79**, 571 (2004).
[33]Z. V. Gabbasova, M. D. Kuz'min, A. K. Zvezdin, I. S. Dubenko, V. A. Murashov, and D. N. Rakov, Phys. Lett. A **158**, 491 (1991).